Control of Tip Leakage Flow in Axial Flow Compressor Cascade by Suction on the Blade Tip

X. Mao, B. Liu[†] and T. Tang

School of Power and Energy, Northwestern Polytechnical University，Xi'an, Shaanxi, 710072，P. R. China

†*Corresponding author email: liubo704@nwpu.edu.cn*

ABSTRACT

One of the important ways of improving axial compressor performance is to control the tip leakage flow near the endwall region. Numerical computations were conducted to investigate the impact of blade tip suction on the axial compressor cascade performance in current paper. Three suction schemes located on the blade tip with different chordwise coverage were investigated in total. The results show that the cascade overall performance can be effectively enhanced by the proper suction scheme on the blade tip and the best scheme should be arranged at slightly downstream of the onset point of the tip leakage vortex (TLV). The control effectiveness and mechanisms are different for the different suction schemes. For the suction scheme covering the starting point of TLV, the onset point of TLV is shifted downstream, while an additional induced leakage flow near the blade leading edge is generated resulting in the increase of mixing loss. It is more effective when the structure of the main TLV is destroyed and divided into different parts by applying the blade tip suction arranged slightly behind the onset point of TLV. In addition, the blade loading is redistributed near the blade tip after the blade tip suction and the total pressure loss caused by the suction slots should also be considered in the design process.

NOMENCLATURE

C	blade chord length	w	local total pressure loss coefficient
Cp	static pressure coefficient	$\overline{w}_{total}$	overall total pressure loss coefficient of cascade
CP	static pressure rise coefficient		
h	blade height	$\overline{w}_{TLF}$	overall total pressure loss coefficient caused by TLF
H	enthalpy		
i	flow incidence	$\overline{w}_{slot}$	overall total pressure loss coefficient caused by suction slot
Ma_1	inlet Mach number		
P	local static pressure	y+	non-dimensional wall distance
P_1	inlet static pressure		
P^*	local total pressure	β_s	blade stagger angle
P_1^*	inlet total pressure	β_{1k}	blade inlet angle
t	blade pitch	β_{2k}	blade outlet angle
U	mean blade speed	β_1	inlet flow angle
V_1	inlet velocity	β_2	outlet flow angle
V_x	inlet axial velocity	ρ	density

1. INTRODUCTION

It is well known that tip leakage flow (TLF) is responsible for the deterioration of efficiency and stall margin in compressors. Generally, the TLF rolls up into a tip leakage vortex (TLV) along the suction surface (SS) near the blade tip and then it moves across the blade passage towards the

pressure surface (PS) of the adjacent blade. Much effort has been made to clarify this complicated flow in the past decades (Inoue *et al*. 1986, 1989; Storer *et al*. 1991; Kang *et al*. 1996; Borello *et al*. 2007; Beselt *et al*. 2014). In order to improve the overall performance and the operational range of the compressor, both passive and active flow control techniques related to TLF have long been hot topics in the development of turbomachinery and continue to attract a great deal of attention. In the passive flow control methods such as casing treatment (Houghton *et al*. 2012; Sakuma *et al*. 2014; Du *et al*. 2016), blade tip winglet (Han *et al*. 2014, 2016) and blade tip modifications (Gourdain *et al*. 2009; Ma *et al*. 2012; Jung *et al*. 2016), the geometrical change always works among the whole operating range and it may lead to a decrease of compressor performance near the design condition. For the active flow control techniques such as plasma actuation (Saddoughi *et al*. 2015; Ashrafi *et al*. 2016), tip injection (Li *et al*. 2015; Grosvenor *et al*. 2015; Khaleghi *et al*. 2016) and casing aspiration (Lee *et al*. 1990; Gmelin *et al*. 2011; Grimshaw *et al*. 2015), however, it can act on the flow fields flexibly either all the time or only when it is needed. As one of the effective active flow control methods, the suction technique attracts the attention from an increasing number of researchers to improve the flow fields in compressors. Additionally, the aspirated flow from the suction slots can provide air for the secondary air system in aircraft engine. Therefore, the suction technique will have a broad application prospect in the future. So far the studies about suction mainly concentrate on the control of the boundary layer separation on the blade SS (Song *et al*. 2006; Guo *et al*. 2010; Shi *et al*. 2015b) or the three-dimensional (3D) separation in the hub corner (Sachdeva *et al*. 2011; Pönick *et al*. 2013; Guo *et al*. 2008; Marsan *et al*. 2015). Apart from some researches about the effects of bleeding system on the compressor performance (Leishman *et al.* 2007a, 2007b, 2007c; Grimshaw *et al*. 2015, 2016), there are only several investigations of suction technique on the control of TLF to improve the compressor performance and stability (Gümmer *et al*. 2008; Dobrzynski *et al*. 2008; Shi *et al*. 2015a). It is found that the flow fields in the tip region and operating range can be improved by the suction on the casing. In addition, very little study has been carried out on the effectiveness of suction located on the blade tip and the corresponding control mechanisms.

To better understand the control mechanisms of blade tip suction and provide reference for the application of suction technique on the advanced aircraft engines, the focus of current paper will be mainly on (1) how to set up the suction slot on the blade tip is the best choice for compressor designers (2) what is the control mechanisms of the different blade tip suction schemes. This paper is organized as follows. Firstly, the studied cascade and computational procedure are provided in Section 2. Then the validation of computational procedure and the arrangement of suction schemes are presented in Section 3 and Section 4 respectively. The numerical results and analysis are shown in Section 5. Finally, a list of conclusions is summarized in Section 6.

1. INVESTIGATED COMPRESSOR CASCADE AND COMPUTATIONAL PROCEDURE

2.1 Cascade Description

A typical high pressure compressor cascade was selected to study the effectiveness of blade tip suction and the corresponding control mechanisms. The original cascade consists of eight blades without tip clearance. Table 1 shows the main parameters of the cascade at the design condition. The ratio of blade tip gap size to the blade height is 1% in the current paper and the two-dimensional cascade configuration is shown in Fig. 1.

Table 1 Cascade design parameters

Parameter	Variable	Value	Unit
No. of blades	-	8	[-]
Blade chord length	C	65	*mm*
Blade height	h	100	*mm*
Blade pitch	t	37.57	*mm*
Aspect ratio	h/C	1.54	[-]
Blade solidity	C/t	1.73	[-]
Blade stagger angle	β_s	21.27	degree
Blade inlet angle	β_{1k}	47.08	degree
Blade outlet angle	β_{2k}	-1.98	degree
Inlet Mach number	Ma_1	0.4	[-]
Flow incidence	i	0	degree
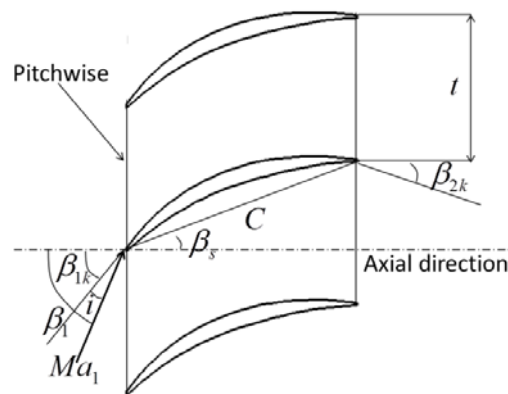
Fig. 1. Two-dimensional cascade configuration.

2.2 Computational Procedure

The simulations were performed based on the three-dimensional (3D) RANS using the CFD software package FINE/Turbo from NUMECA International. It solves the compressible 3D RANS equations using an explicit time marching four-step Runge–Kutta scheme. The equations are discretized in space by using a second order cell-centered explicit finite volume scheme. One equation turbulence model of Spalart and Almaras (S-A) was selected for the computations. The nonslip and adiabatic conditions were applied on all walls. Absolute total temperature, total pressure and inlet flow angle were given at the inlet boundary of the blade passage, and the static pressure at the outlet was given according to the desired mass flow condition. To ensure the suction flow ratio (SFR, which is defined as the ratio of aspirated mass flow rate to the cascade inlet mass flow rate), a designated mass flow condition at the suction slot outlet was adopted.

The computational mesh was generated by AUTOGRID5. Type of structured O4H topology was adopted for the main blade passage, and the blade tip gap was modeled with butterfly mesh topology. The computational domain starts from 100%C upstream from the blade leading edge (LE) to 150%C downstream from the blade trailing edge (TE).

Firstly, the error analysis on the mesh density is conducted to ensure the accuracy of the computational method used in the current paper. Fig. 3 shows the change of loss coefficient with different numbers of nodes in tip gap with the grid density of about 1.21 million. We can see that the influence of node number in tip gap becomes unobvious from 17. The variation trend of the cascade performance with different grid numbers of the blade passage is plotted in Fig. 3, in which the nodes number in the tip gap is set as 17. One can observe that the loss only decreases slightly when the grid density is larger than 1.21 million. Thus, a total mesh number of about 1.21 million with 17 nodes in the tip clearance is determined for the blade passage in the simulations.

The computational mesh near the blade SS and endwall (EW) together with the enlarged views of the mesh near the blade tip is presented in Fig. 4.The minimum grid spacing on the solid wall was 5×10^{-6} m to predicate the viscous fluxes near the walls, which gives the parameter of y+ less than 4.5 shown as Fig. 5. Therefore, the distribution of dimensionless wall distance satisfies the requirement of the S-A turbulence model, i.e., the value of y+ is no more than 10.
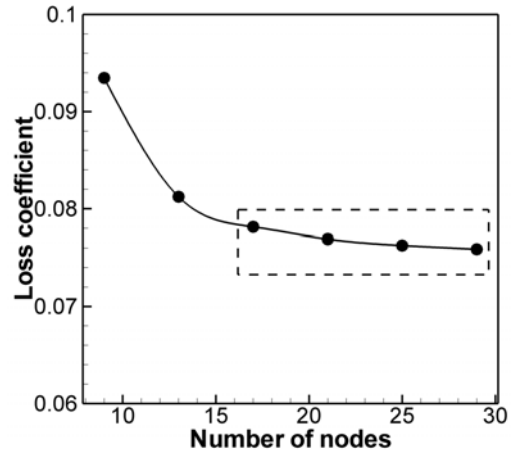

Fig. 2. Cascade performance with different number of nodes in tip gap.
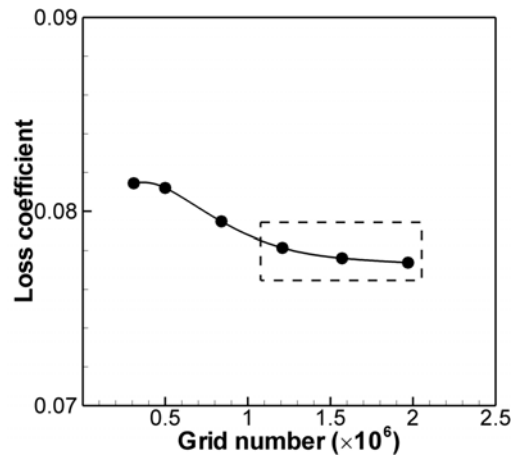

Fig. 3. Cascade performance with different number of grid.

3. VALIDATION OF COMPUTATIONAL PROCEDURE

To ensure the accuracy of the computational procedure, the comparison of the static pressure coefficient at mid-span between the experiments and computations for the studied cascade without tip clearance size at 4° incidence is shown in Fig. 6. The static pressure coefficient is defined as the ratio of local static pressure to the inlet total pressure. One can see that the agreement between experiments and computational results is generally well. As is known to all that the flow patterns are very complicated in the hub corner and the tip region. Thus, it is needed to guarantee the capability of computational procedure to predict the complicated flow structures near the EW. Due to the lack of adequate experimental results for the investigated cascade with tip clearance, another cascade denoted as Cascade 2 is selected to check the reliability of the computational procedure. Table 2 shows the design parameters of Cascade 2 at the
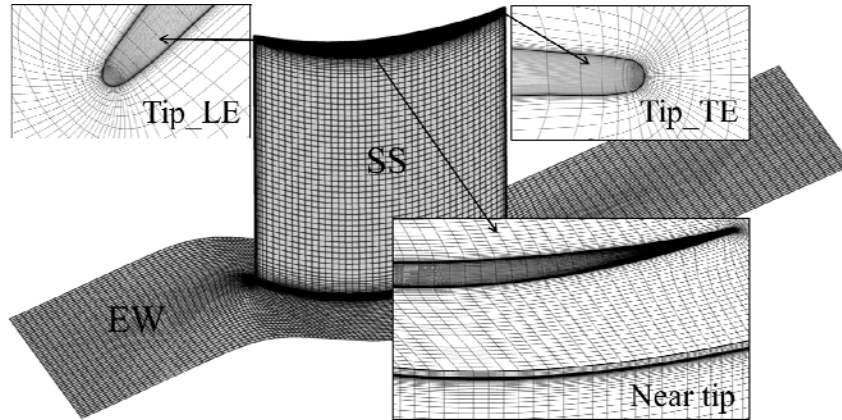
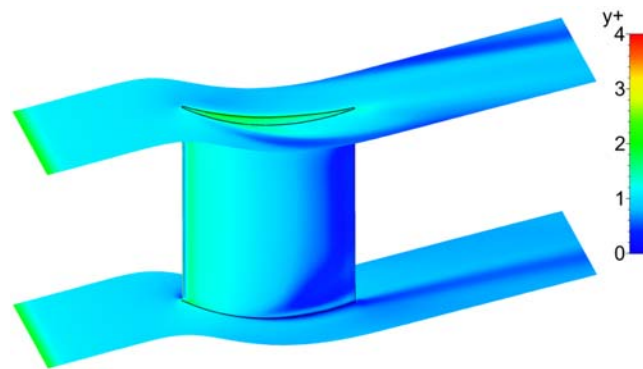**Fig. 4. Computational mesh near the blade SS and EW.**

**Fig. 5. Distribution of dimensionless wall distance on the EW and blade SS.**

Table 2 Design parameters of Cascade 2

Parameter	Variable	Value	Unit
No. of blades	-	7	*[-]*
Blade chord length	C	65	*mm*
Blade height	h	100	*mm*
Blade pitch	t	43.92	*mm*
Aspect ratio	h/C	1.54	*[-]*
Blade solidity	C/t	1.48	*[-]*
Blade stagger angle	β_s	27	*degree*
Blade inlet angle	β_{1k}	48	*degree*
Blade outlet angle	β_{2k}	12	*degree*
Inlet Mach number	Ma_1	0.5	*[-]*
Flow incidence	i	0	*degree*

aerodynamic design condition. Fig. 7 compares the numerical and experimental results of the flow patterns near the walls at the design point in Cascade 2. Both the grid number and mesh topology in the simulation of Cascade 2 are the same as the investigated cascade in this paper. It can be seen that the predicted flow pattern on the SS matches the experimental result very well except for its slightly larger separation area. On the EW, although the separation line (SL) originating from the saddle point of S2 is closer to the blade SS in the computation and the trajectory of horseshoe vortex on the blade pressure surface (HVps) turns more sharply in the experiment, the critical points

(i.e., saddle point, node or focus according to the topological rules) are well captured. Thus, the agreement between simulation and experiment is generally good, which gives us confidence in applying the computational procedure. It should be mentioned that the experiments of the two investigated cascades were both conducted in a high-subsonic cascade wind tunnel at the National Defense Aerodynamics Laboratory of Airfoil and Cascade in Northwestern Polytechnical University (NWPU) of China. Due to the restriction of the article length, the details of the experimental process are not presented here and more details of the experiments can be found in the Reference (Bo, 2011).
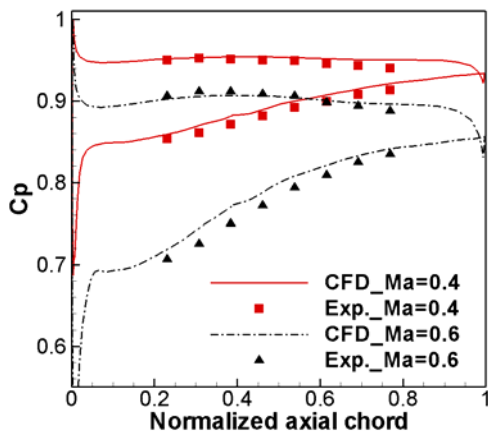
Fig. 6. *Cp* **distributions of numerical and experimental results of the original cascade at mid-span.**

4. SUCTION SCHEME ARRANGEMENTS

Simulations of the basic flow configuration were carried out first and the results showed that the onset points of the TLV are located at about 25% and 13% axial chord at the incidence of 0° and 4° respectively. In this paper, three different suction schemes, denoted as Slot A, Slot B and Slot C respectively, were investigated according to the onset point of TLV. The suction slots were set up on the blade tip along the camber line of the blade profile, and the center of the slots coincides with the camber line.

The slot arrangements of suction schemes are shown in Fig. 8, in which the enlarged views of the mesh of Slot B is also presented. The coverage extents of the three suction schemes are 8%-33% axial chord (Slot A), 33%-59% axial chord (Slot B), and 59%-86% axial chord (Slot C) respectively. Both the height and width of the slots are the same of 1mm. Therefore, we can see that starting point of the TLV is within the coverage of Slot A.

The mesh of the suction slots was a structured H grid generated by the software of IGG with 33 grid points in streamwise direction, and 13 grid points in both pitchwise and spanwise direction. The grids of the suction slots were connected with the blade flow passage by the full non-matching connection technology.

5. RESULTS AND DISCUSSION

The influence of the suction schemes on the cascade overall performance is analyzed first. The local total pressure loss coefficient is defined as Eq. (1), and the measurement plane is located at about 50% chord downstream of the blade TE. The overall loss coefficient is calculated by the mass-weight average of the local total pressure loss coefficient at the measurement plane.

$$w = \frac{P_1^* - P^*}{P_1^* - P_1} \tag{1}$$

The change of the overall loss coefficient mainly caused by TLF at the measurement plane with SFR is shown in Fig. 9. The overall loss mainly caused by TLF is calculated from the mid-span to the casing. One can see that the overall loss coefficient is increased slightly at SFR of 0.0% for the three schemes due to the interaction between the suction slot and the local TLF. For the scheme of Slot A, the overall loss coefficient can only be reduced remarkably when the SFR is higher than about 0.5%. The reduction of overall loss in Slot C is the least significant at the SFR of about 0.7%. Compared with Slot A and Slot C, Slot B is the best suction scheme for both the flow conditions. The overall loss coefficient drops gradually with the increasing of SFR, and the decreasing speed increases obviously from the SFR of about 0.5%. At the SFR of about 0.7%, the overall loss in Slot B is decreased by about 13.6% and 9.6% at the incidence of 0° and 4° respectively. The results of the basic flow analysis show that the starting points of TLV are located at about 25% and 13% axial chord for at the incidence of 0° and 4° respectively and both the onset locations of TLV are within the covering range of Slot A. Generally, the onset point of TLV corresponds to the maximum blade loading near the tip. The suction scheme covering the onset point of TLV may increase the complexity of the local flow field due to the interaction between the suction slot and the local TLF, which contributes the increasing of the slot-related loss. From Fig. 9, one can also see that the total pressure loss is increased slightly at the lower SFR for Slot A, especially at 0° incidence. Therefore, the optimum suction scheme on the blade tip should be located slightly downstream of the onset point of TLV.
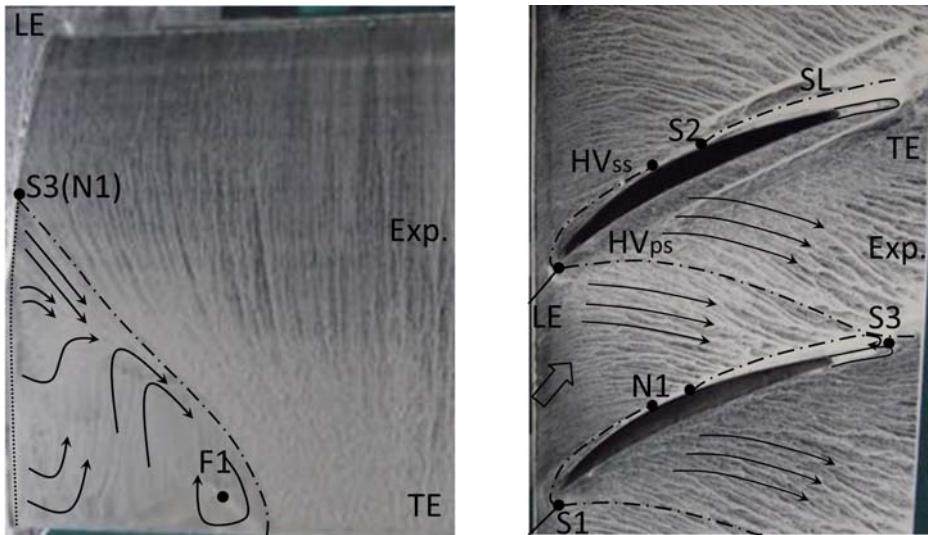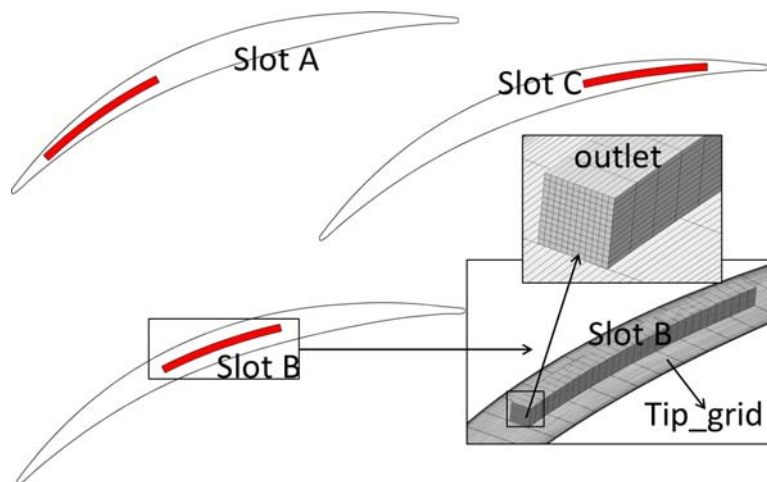
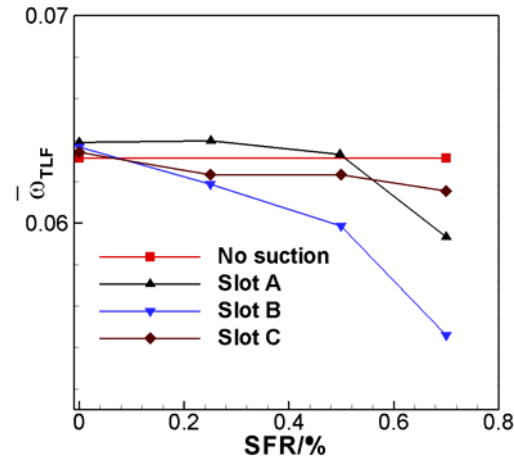(a) Experimental results of flow pattern on SS and EW
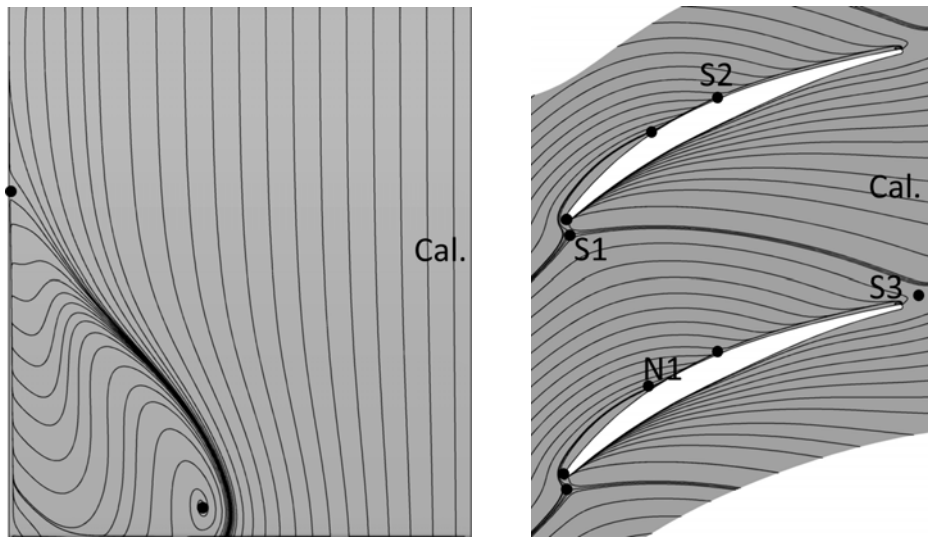
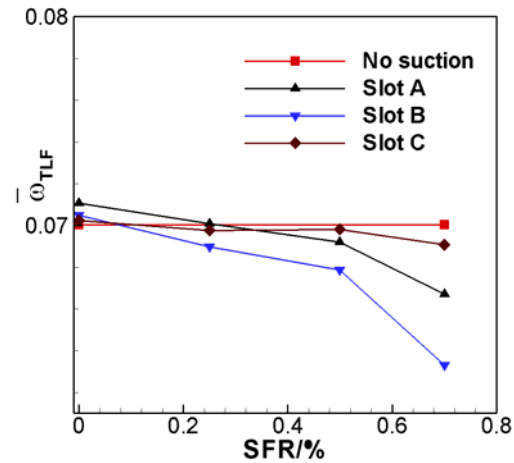(b) Numerical results of flow pattern on SS and EW

Fig. 7. Comparisons of numerical and experimental results of the flow patterns in Cascade 2.

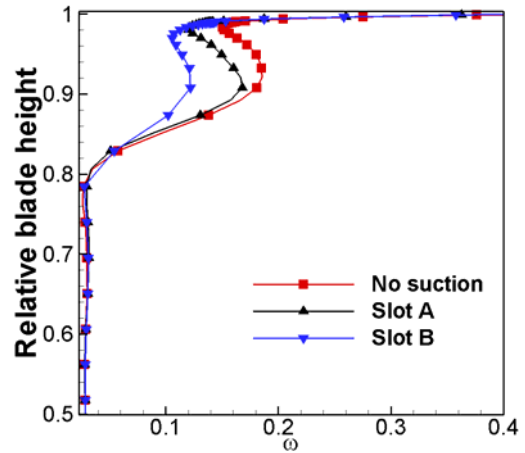**Fig. 8. Suction slot arrangements (viewed from the hub side).**

(a) i=0°

Fig. 10. Radial distribution of pitch-averaged total pressure loss coefficient.

(b) i=4°

Fig. 9. Variation of the overall total pressure loss coefficient mainly caused by TLF.

In the following analysis, suction schemes of Slot A and Slot B will be used to further study the change of flow structures in the blade tip region and the corresponding control mechanisms with 0°incidence at the SFR of about 0.7%. The radial distributions of the pitch-averaged total pressure loss coefficient are presented in Fig. 10. It can be seen that the blade tip suction has an obvious influence on the flow filed in the tip region. The loss coefficients of the two suction schemes are both decreased after suction and the scheme of Slot B shows more effective. Additionally, the spanwise location of the loss peak corresponding to the TLV core at about 90% span almost remains unchanged after suction, which indicates that the blade tip suction has little impact on the radial location of the TLV core. Therefore, the reduction of the intensity and pitchwise extent of TLV is probably the main contribution for the improvement of cascade performance.

Figure 11 shows the TLV trajectory in the two suction schemes. The trajectory of TLV is presented by a black dash-dotted line along the static pressure trough on the casing wall. It can be seen that there is a local lower static pressure zone due to the suction effect, and both the TLV trajectories of the two suction schemes are changed obviously after suction. In Fig. 11 (b), the TLV trajectory on the casing shows that the onset point of TLV is shifted downstream obviously. In addition, the blade loading near the beginning of the slot denoted by red circle is increased due to the suction effect, which may induce a stronger local leakage flow. For the scheme of Slot B, the original main TLV is divided into two parts after suction. The front part TLV becomes closer to the SS and it starts from almost the same location as the original TLV, while the starting point of the rear part TLV is near the blade TE. Finally, the two parts of TLV merge together near the blade TE. Therefore, we can see that the control mechanisms of two suction schemes are different in improving the cascade performance. Compared with the original cascade without suction, the influence range of TLV in pitchwise direction is decreased obviously. Therefore, the overall strength and impact of TLV are reduced after the suction in both suction schemes.
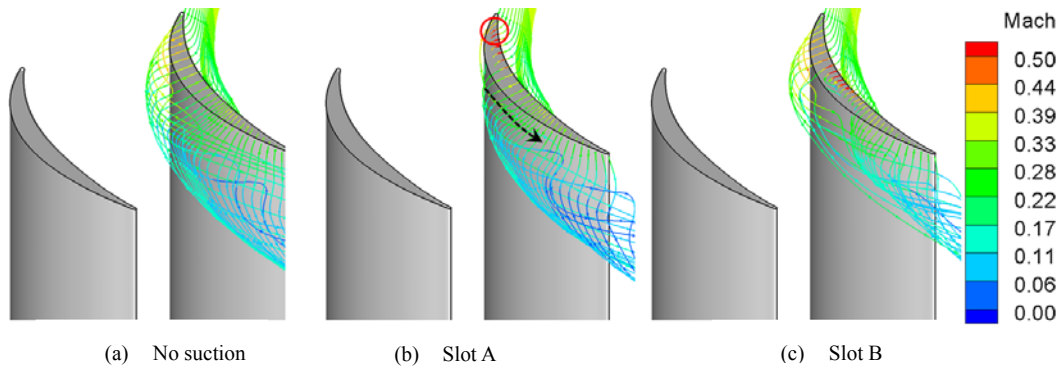
The 3D streamlines released from near blade tip, mid-gap and near casing for the suction schemes of Slot A and Slot B are shown in Figs. 12-14 respectively. It can be seen that the flow structures of TLV are changed obviously in both suction schemes and the extent of TLV both in pitchwise and spanwise direction is reduced more significantly in Slot B. After the suction of Slot B, the TLV is divided into two parts. The strength of the primary TLV corresponding to the front part is reduced remarkably as the tip clearance flow slightly behind the onset point of TLV is removed.

143
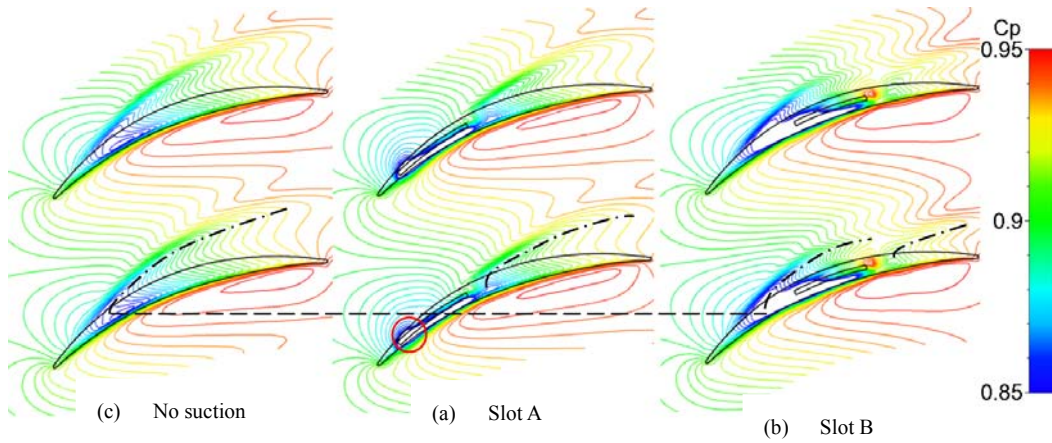
Fig. 11. Static pressure coefficient distributions on the casing.

(a)   No suction   (b)   Slot A   (c)   Slot B

Fig. 12. 3D streamlines released from near blade tip.

(a)   No suction   (b)   Slot A   (c)   Slot B
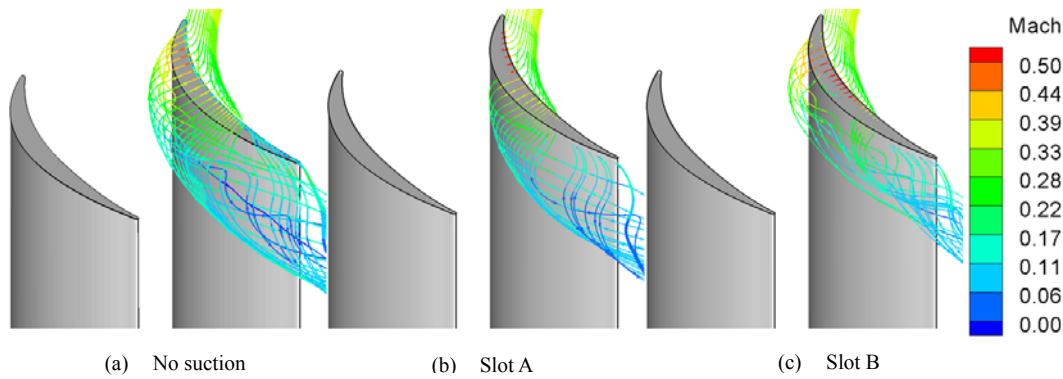
Fig. 13. 3D streamlines released from the mid-gap.

Additionally, the impact of the rear part TLV is also less significant on the performance due to the weak intensity of TLV near blade TE. The 3D streamlines released from different tip gap height all show that the strength of the TLV is reduced obviously after the suction of Slot B. For Slot A, the Figures show that the tip clearance flow around the original onset point of TLV is sucked away directly from the suction slot. Thus, the onset location of TLV is shifted downstream and the TLV becomes more close to the SS, which indicates the influence of the TLV is decreased after the suction, which is

consistent with the change of TLV trajectory on the casing shown as Fig. 11. In addition, the variation of TLF structures leaked from different tip gap height is different after the suction of Slot A. From Figs. 13 and 14, it can be seen that there is an additional induced leakage flow denoted by black dashed line with arrow near the blade LE and it is finally rolled into the main TLV. Due to the suction effect, the blade loading near LE is increased slightly shown as Fig. 15 (b) and there is a tendency of local casing boundary layer to move toward lower blade span, which may be responsible for the
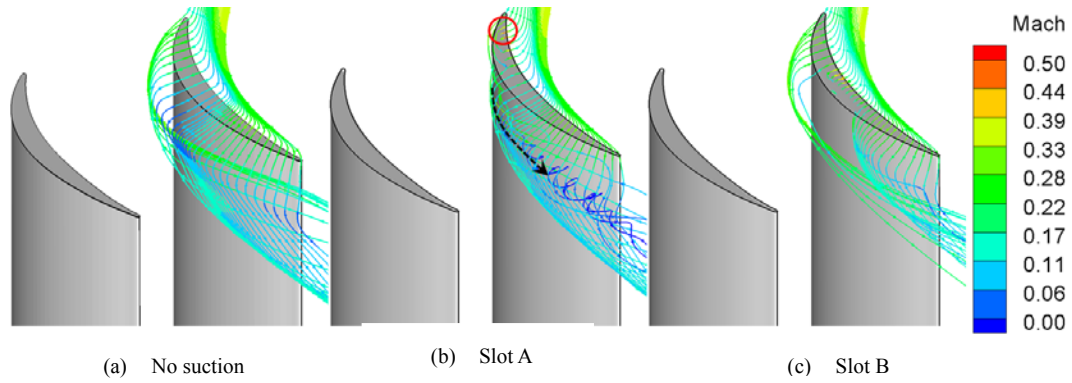
(a) No suction   (b) Slot A   (c) Slot B

Fig. 14. 3D streamlines released from near casing.
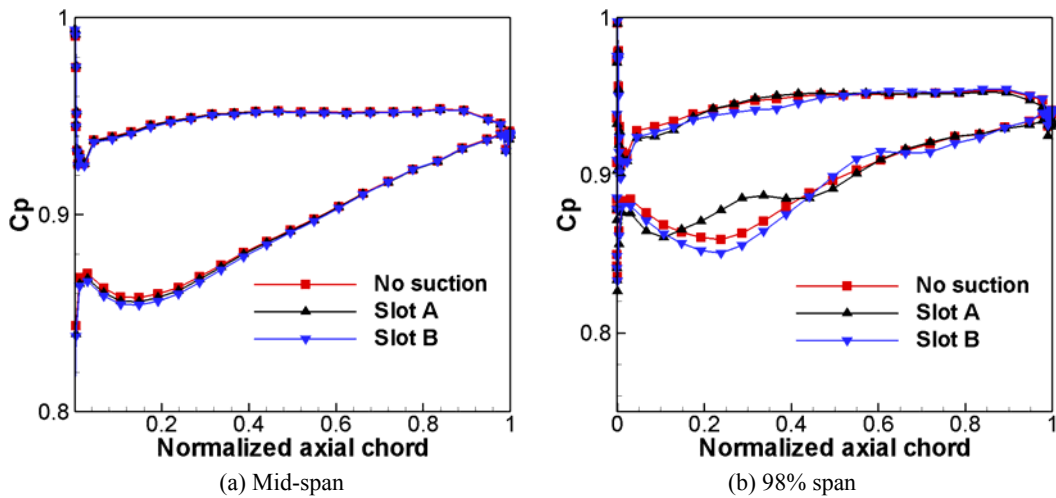

(a) Mid-span   (b) 98% span

Fig. 15. Static pressure coefficient distributions at mid-span and 98% blade span.

appearance of the additional induced leakage flow. Although the extent of main TLV is reduced, the occurrence of induced leakage flow would result in the additional mixing loss in the process of downstream movement. According to the 3D streamlines released from near casing shown as Fig. 14(b), one can see that the induced leakage flow with higher intensity merges with the main TLV obviously. Therefore, the optimal suction scheme on the blade tip should be arranged slightly downstream of the onset point of TLV. In this way, the main TLV is divided into two parts with weaker strength and the corresponding mixing loss can be decreased significantly.

Figure15 shows the static pressure coefficient distributions at the mid-span and about 98% blade span. One can see that blade tip suction has remarkable influence on the flow field near the blade tip and little impact on the flow near the mid-span. Fig. 15 (b) shows that the blade tip suction redistributes the blade tip loading along the chord, and the static pressure on the blade suction side within and around the coverage of the slots changes obviously. The static pressure slightly in the front

and behind of the suction slot is decreased, which results in an enhancement of the local blade loading. Generally, the strength of TLV is in proportion to the loading near the blade tip, and the TLV often starts at the maximum loading of the blade. We can observe that the maximum blade loading position moves to about 45% axial chord in Slot A, which is consistent with the downstream movement of the starting location of TLV. The enhancement of the blade loading behind the suction slot corresponds to the happening of the new TLV in Slot A and the rear part TLV in Slot B respectively after suction. The decreasing of the static pressure in front of the slot is probably due to the reason that the local leakage flow is accelerated by the suction effect. For Slot A, the reduction of the static pressure on suction side in front of the slot is responsible for the occurrence of the local induced leakage flow near blade LE. Actually, the blade loading in front of the slot is also increased slightly after the suction of Slot B shown as Fig. 15 (b), which indicates the intensity of front part TLV is increased to some extent. However, it has no significant influence on the generation of mixing

(a)   No suction   (b)   Slot A   (c)   Slot B
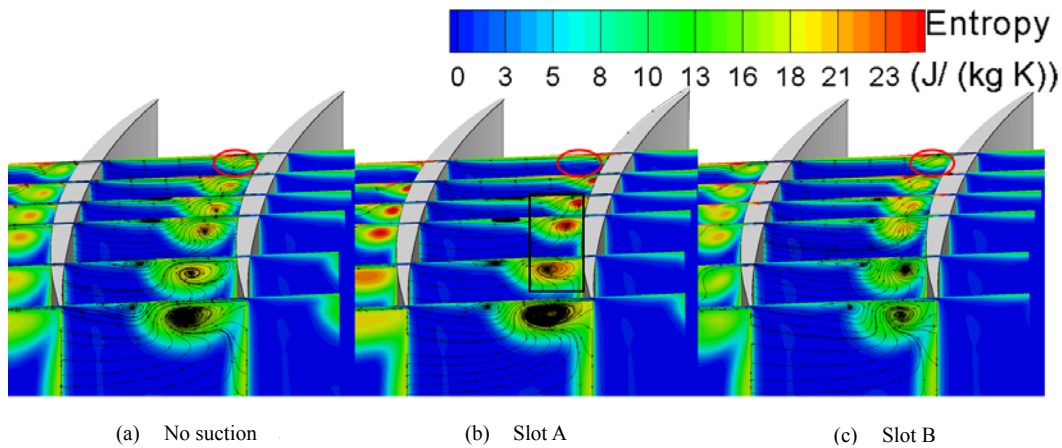
Fig. 16. Entropy contours and streamlines on different axial slices.

loss between the two parts of TLV due to the weaker strength of the rear part TLV and the shorter mixing distance. In addition, the blade loading within the slot coverage is reduced after suction due to the reason that the local tip leakage flow is removed.

Previous studies show that the TLF dominates the tip flow field, and there is usually an interaction between the tip passage vortex and TLV. To obtain a better insight into the control mechanisms, the development of flow fields in the tip region will be studied after suction. The entropy contours and surface streamlines on six axial planes (30%, 40%, 50%, 60, 80%, and 100% axial chord) are presented in Fig. 16. Compared with the cascade without suction, one can see from the section at the blade TE that the extent and strength of TLV are reduced obviously in Slot B, and the corresponding entropy range decreases remarkably. However, the control effectiveness is less significant in Slot A. From the plane at 30% axial chord, it can be seen that the high entropy zone due to TLV almost disappears after the suction of Slot A, which corresponds to the downstream shifting of the onset point of TLV. Besides, we can also observe that the entropy marked by black rectangle increases slightly in Slot A. It is probably because that the blade loading is enhanced in front of the slot shown as Fig. 15 (b), which results in the happening of induced leakage flow and the generation of the mixing loss. In addition, it can be seen that the location of tip passage vortex moves more close to the blade SS due to the reduction of the TLV extent after the suction of Slot B. Compared with the Slot A from the plane at the blade TE, one can also observe that the location of the vortex core is much closer to the blade suction side in Slot B, which contributes to the reduction of flow

blockage in the tip regione. Therefore, we can conclude that it is more efficient if the structure of main TLV is destroyed and divided into different parts by applying the blade tip suction, and the suction slot should be arranged at slightly downstream of the onset point of TLV.

Generally, there is an additional loss caused by the suction slot in the suction schemes and it should be considered in evaluating the effectiveness of the suction system. In the simulations of the suction schemes, the inlet mass flow rate is a sum of the outlet mass flow rate and the suction flow rate. Thus, the total loss coefficient is defined in Eq. (2). The slot-related loss is computed according to the definition of suction-loss coefficient by Evans *et al.* (2010).

$$\overline{w}_{total} = (1 - SFR)\,\overline{w}_{TLF} + \overline{w}_{slot} \tag{2}$$

The changes of the slot-related total pressure loss coefficient and total loss coefficient in Slot B at 0° incidence are plotted in Fig. 17. From Fig. 17 (a), it can be seen that the slot-related loss increases gradually with the SFR, while the growth speed is more and more slowly. Thus, the loss coefficient caused by the suction slot is non-negligible in the compressors with suction control system. In Fig. 17 (b), we can see that the total loss begins to decrease from the SFR of about 0.7%. Therefore, the cascade overall performance can only be improved when the SFR is high enough. The total loss coefficient in Slot B can be reduced by about 1.9% at the incidence of 0° with SFR of about 0.7% when considering the slot-related loss. Actually, the slot-related loss coefficient can be further decreased by optimizing the configuration of the slots. Therefore, it is important to obtain the proper suction scheme and slot geometry during the design of aspirated compressors.
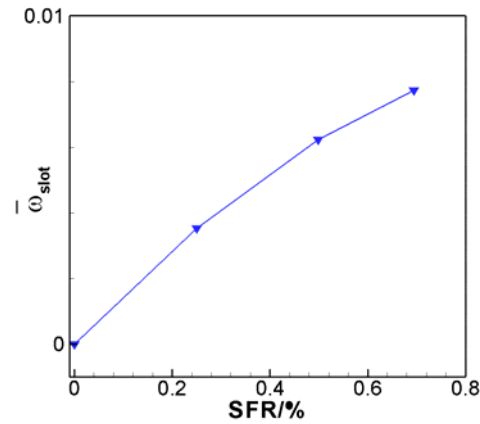
(a) slot-related total pressure loss coefficient
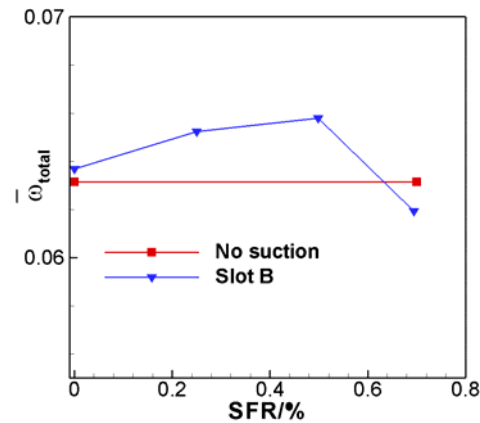
(b) overall total pressure loss coefficient

Fig. 17. Variation of the slot-related total pressure loss coefficient and overall total pressure loss coefficient in Slot B at 0° incidence.

Except for the reduction of overall total pressure loss, the gain in static pressure rise for the mainstream is another factor to evaluate the effectiveness of blade tip suction. Then an approximate calculation of the increase in static pressure rise is conducted to compare the obtained gain with the energetic cost of the suction in the scheme of Slot B. The calculation method is the same as the approach used by Gbadebo *et al.* (2008).

At 0° incidence with the SFR of about 0.7%, the average outlet flow angle β_2 is about 7°. Assuming a repeating stage with mean flow coefficient V_x/U of 0.5, then

$$\Delta H_0 / U^2 = V_x(\tan\beta_1 - \tan\beta_2)/U = 0.4763 \quad (3)$$

Then the lost work caused by the bleeding air can be given as

$$(SFR)\Delta H_0 / U^2 = 0.007 \times 0.4763 = 0.0033 \quad (4)$$

Therefore the static pressure reduction due to the bleeding air is about

$$\Delta P_0 = 0.0033\rho U^2 \quad (5)$$

The cascade static pressure rise is specified in terms of inlet dynamic pressure. The inlet velocity

$$V_1 = UV_x / (U\cos\beta_1) = 0.5U / \cos\beta_1 = 0.7342U \quad (6)$$

Then the inlet dynamic head is given by

$$1/2 \times \rho V_1^2 = 0.2696\rho U^2 \quad (7)$$

Therefore, the increase in static pressure of the cascade

$$\Delta P = (CP_{SlotB} - CP_{No\,suction}) \times 0.2696\rho U^2 = 0.00496\rho U^2 \quad (8)$$

One can see that the increase in static pressure is about 1.5 times the static pressure reduction due to the bleeding air. Actually, the gains of the mainflow in terms of total pressure loss reduction and the increase in static pressure rise can be further enhanced when the benefits from the second use of the bleeding air are considered. Therefore, the blade tip suction is an effective flow control technique to improve the cascade performance.

6. CONCLUSIONS

In this paper, the effectiveness of blade tip suction and the corresponding control mechanisms are studied numerically. The conclusions are shown as below.

(1) The overall performance of the cascade can be obviously enhanced by the proper suction scheme on the blade tip. A best suction scheme should be arranged at slightly downstream of the onset point of TLV. At the SFR of about 0.7%, the total loss coefficient is reduced by about 13.6% and 1.9% without and with considering the slot-related loss respectively at 0° incidence for the best blade tip suction scheme.

(2) The control mechanisms are different for the different tip suction schemes. For the suction scheme covering the starting location of TLV, the onset point of TLV is shifted downstream. However, an additional induced leakage flow near LE is generated resulting in the increase of mixing loss. When the suction scheme is arranged slightly behind the starting point of TLV, the original main TLV structure is separated into two parts with weaker strength and the corresponding mixing loss can be decreased significantly. Therefore, it is more efficient if the structure of main TLV is destroyed and divided into different parts by applying the blade tip suction.

(3) The blade loading along the chord near blade tip is redistributed after the suction, and its change corresponds to the intensity and structure

variation of the TLV. The loss coefficient caused by the suction slot is non-negligible, and it is important to obtain the proper suction scheme and slot geometry during the design of aspirated compressors.

ACKNOWLEDGEMENTS

REFERENCES

Ashrafi, F., M. Michaud and H. D. Vo (2016). Delay of rotating stall in compressors using plasma actuators. *Journal of Turbomachinery* 138(9), 091009.

Beselt, C., M. Eck and D. Peitsch (2014). Three-dimensional flow field in highly loaded compressor cascade. *Journal of Turbomachinery* 136(10), 101007.

Bo, X. F. (2011) *The experimental and numerical study of the characteristics of compressor cascade boundary layer*. Ph. D. thesis, the Northwestern Polytechnical University, xi'an China.

Borello, D., K. Hanjalic and F. Rispoli (2007). Computation of tip-leakage flow in a linear compressor cascade with a second-moment turbulence closure. *International Journal of Heat and Fluid Flow* 28(4), 587-601.

Dobrzynski, B., H. Saathoff, G. Kosyna, C. Clemen and V. Gummer (2008). Active flow control in a single-stage axial compressor using tip injection and endwall boundary layer removal. *ASME GT2008-50214.*

Du, J., J. Li., L.Gao, F. Lin and J. Chen (2016). The Impact of Casing Groove Location on Stall Margin and Tip Clearance Flow in a Low-Speed Axial Compressor. *Journal of Turbomachinery* 138(12), 121007.

Evans, S., H. Hodson, T. Hynes and C. Wakelam (2010). Flow control in a compressor cascade at high incidence. *Journal of Propulsion and Power* 26(4), 828-836.

Gbadebo, S. A., N. A. Cumpsty and T. P. Hynes (2008). Control of three-dimensional separations in axial compressors by tailored boundary layer suction. *Journal of Turbomachinery* 130(1), 011004.

Gmelin, C., F. Thiele, K. Liesner and R. Meyer (2011). Investigations of secondary flow suction in a high speed compressor cascade. *ASME GT2011-46479.*

Gourdain, N. and F. Leboeuf (2009). Unsteady simulation of an axial compressor stage with casing and blade passive treatments. *Journal of turbomachinery* 131(2), 021013.

Grimshaw, S. D., G. Pullan and T. P. Hynes (2016). Modeling Nonuniform Bleed in Axial Compressors. *Journal of Turbomachinery* 138(9), 091010.

Grimshaw, S. D., G. Pullan and T. Walker (2015). Bleed-induced distortion in axial compressors. *Journal of Turbomachinery* 137(10), 101009.

Grosvenor, A. D., G. S. Rixon, L. M. Sailer, M. A. Matheson, D. P. Gutzwiller, A. Demeulenaere, M. Gontier and A. J. Strazisar (2015). High resolution rans nonlinear harmonic study of stage 67 tip injection physics. *Journal of Turbomachinery* 137(5), 051005.

Gümmer V, M. Goller and M. Swoboda (2008). Numerical investigation of end wall boundary layer removal on highly loaded axial compressor blade rows. *Journal of Turbomachinery* 130(1), 011015.

Guo, S, H. Lu, F. Chen and C. Wu (2008). Vortex control and aerodynamic performance improvement of a highly loaded compressor cascade via inlet boundary layer suction. *Experiments in fluids* 54(7), 1-11.

Guo, S., S. Chen, Y. Song, Y. Song and F. Chen. (2010). Effects of boundary layer suction on aerodynamic performance in a high-load compressor cascade. *Chinese Journal of Aeronautics* 23(2), 179-186.

Han, S. and J. Zhong (2016). Effect of blade tip winglet on the performance of a highly loaded transonic compressor rotor. *Chinese Journal of Aeronautics* 29(3), 653-661.

Han, S., J. Zhong, H. Lu, X. Kan and L. Yang (2014). Effect of winglet geometry arrangement and incidence on tip clearance control in a compressor cascade. *Journal of Thermal Science* 23(4), 381-390.

Houghton, T. and I. Day (2012). Stability enhancement by casing grooves: The importance of stall inception mechanism and solidity. *Journal of Turbomachinery* 134(2), 021003.

Inoue, M. and M. Kuroumaru (1989). Structure of tip clearance flow in an isolated axial compressor rotor. *Journal of Turbomachinery* 111(3), 250-256.

Inoue, M., M. Kuroumaru and M. Fukuhara (1986). Behavior of Tip Leakage Flow Behind an Axial Compressor Rotor. *Journal of Engineering for Gas Turbines and Power* 108(1), 7-14.

Jung, Y. J., H. Jeon, Y. Jung, K. J. Lee and M. Choi (2016). Effects of recessed blade tips on stall

margin in a transonic axial compressor. *Aerospace Science and Technology* 54, 41-48.

Kang, S. and C. Hirsch (1996). Numerical simulation of three-dimensional viscous flow in a linear compressor cascade with tip clearance. *Journal of Turbomachinery* 118(3), 492-502.

Khaleghi, H., M. A. S. Dehkordi and A. M. Tousi (2016). Role of tip injection in desensitizing the compressor to the tip clearance size. *Aerospace Science and Technology* 52, 10-17.

Lee, N. K. W. and E. M. Greitzer (1990). Effects of endwall suction and blowing on compressor stability enhancement. *Journal of Turbomachinery* 112(1), 133-144.

Leishman, B. A., N. A. Cumpsty and J. D. Denton (2007a). Effects of bleed rate and endwall location on the aerodynamic behavior of a circular hole bleed off-take. *Journal of Turbomachinery* 129(4), 645-658.

Leishman, B. A., N. A. Cumpsty and J. D. Denton (2007b). Effects of inlet ramp surfaces on the aerodynamic behavior of bleed hole and bleed slot off-take configurations. *Journal of Turbomachinery* 129(4), 659-668.

Leishman, B. A., N. A. Cumpsty and J. D. Denton (2007c). Mechanism of the interaction of a ramped bleed slot with the primary flow. *Journal of Turbomachinery* 129(4), 669-678.

Li, J., F. Lin, Z. Tong, C. Nie and J. Chen (2015). The dual mechanisms and implementations of stability enhancement with discrete tip injection in axial flow compressors. *Journal of Turbomachinery* 137(3), 031010.

Ma, H., J. Zhang, J. Zhang and Z. Yuan (2012). Experimental study of effects of grooved tip clearances on the flow field in a compressor cascade passage. *Journal of Turbomachinery* 134(5), 051012.

Marsan, A., I. Trébinjac, S. Coste and G. Leroy (2015). Influence of unsteadiness on the control of a hub-corner separation within a radial vaned diffuser. *Journal of Turbomachinery* 137(2), 021008.

Pönick, S., D. Kožulović, R. Radespiel, B. Becker and V. Gümmer (2013). Numerical and experimental investigations of a compressor cascade flow with secondary air removal. *Journal of Turbomachinery* 135(2), 021030.

Sachdeva, A. and F. Leboeuf (2011). Topological studies of three-dimensional flows in a high pressure compressor stator blade row without and with boundary layer aspiration. *Chinese Journal of Aeronautics* 24(5), 541-549.

Saddoughi, S., G. Bennett, M. Boespflug, S. L. Puterbaugh and A. R. Wadia (2015). Experimental investigation of tip clearance flow in a transonic compressor with and without plasma actuators. *Journal of Turbomachinery* 137(4), 041008.

Sakuma, Y., T. Watanabe, T. Himeno, D. Kato, T. Murooka and Y. Shuto (2014). Numerical analysis of flow in a transonic compressor with a single circumferential casing groove: influence of groove location and depth on flow instability. *Journal of Turbomachinery* 136(3), 031017

Shi, L., B. Liu, Z. Na, X. Wu and X. Lu (2015a). Experimental investigation of a counter-rotating compressor with boundary layer suction. *Chinese Journal of Aeronautics* 28(4), 1044-1054.

Shi, Y., J. Bai, J. Hua and T. Yang (2015b). Numerical analysis and optimization of boundary layer suction on airfoils. *Chinese Journal of Aeronautics* 28(2), 357-367.

Song, Y., F. Chen, J. Yang and Z. Wang (2006). A numerical investigation of boundary layer suction in compound lean compressor cascades. *Journal of Turbomachinery* 128(2), 357-366.

Storer, J. A. and N. A. Cumpsty (1991). Tip leakage flow in axial compressors. *Journal of Turbomachinery* 113(2), 252-259.